Open Research Online

The Open University's repository of research publications
and other research outputs

# The chlorine isotopic composition of the Moon: Insights from melt inclusions

Journal Item

How to cite:

Stephant, Alice; Anand, Mahesh; Zhao, Xuchao; Chan, Queenie; Bonifacie, Magali and Franchi, Ian (2019). The chlorine isotopic composition of the Moon: Insights from melt inclusions. Earth and Planetary Science Letters, 523 (Early Access).

For guidance on citations see FAQs.

© 2019 The Authors

Version: Version of Record

Link(s) to article on publisher's website:
http://dx.doi.org/doi:10.1016/j.epsl.2019.115715

Copyright and Moral Rights for the articles on this site are retained by the individual authors and/or other copyright owners. For more information on Open Research Online's data policy on reuse of materials please consult the policies page.

oro.open.ac.uk

Earth and Planetary Science Letters 523 (2019) 115715

Contents lists available at ScienceDirect

Earth and Planetary Science Letters

www.elsevier.com/locate/epsl

# The chlorine isotopic composition of the Moon: Insights from melt inclusions

Alice Stephant [a,*], Mahesh Anand [a,b], Xuchao Zhao [a], Queenie H.S. Chan [a], Magali Bonifacie [c], Ian A. Franchi [a]

[a] School of Physical Sciences, The Open University, Milton Keynes, MK7 6AA, UK
[b] Department of Earth Sciences, The Natural History Museum, London, SW7 5BD, UK
[c] Institut de Physique du Globe de Paris, Sorbone Paris Cité, Université Paris Diderot, UMR7154 CNRS, F-75005 Paris, France

ARTICLE INFO

*Article history:*
Received 22 November 2018
Received in revised form 7 July 2019
Accepted 15 July 2019
Available online xxxx
Editor: R. Dasgupta

*Keywords:*
Moon
melt inclusion
NanoSIMS
chlorine isotopes

ABSTRACT

The Moon exhibits a heavier chlorine (Cl) isotopic composition compared to the Earth. Several hypotheses have been put forward to explain this difference, based mostly on analyses of apatite in lunar samples complemented by bulk-rock data. The earliest hypothesis argued for Cl isotope fractionation during the degassing of anhydrous basaltic magmas on the Moon. Subsequently, other hypotheses emerged linking Cl isotope fractionation on the Moon with the degassing during the crystallization of the Lunar Magma Ocean (LMO). Currently, a variant of the LMO degassing model involving mixing between two end-member components, defined by early-formed cumulates, from which mare magmas were subsequently derived, and a KREEP component, which formed towards the end of the LMO crystallization, seems to reconcile some existing Cl isotope data on lunar samples. To further ascertain the history of Cl in the Moon and to investigate any evolution of Cl during magma crystallization and emplacement events, which could help resolve the chlorine isotopic variation between the Earth and the Moon, we analysed the Cl abundance and its isotopic composition in 36 olivine- and pyroxene-hosted melt inclusions (MI) in five Apollo basalts (10020, 12004, 12040, 14072 and 15016). Olivine-hosted MI have an average of $3.3 \pm 1.4$ ppm Cl. Higher Cl abundances (11.9 ppm on average) are measured for pyroxene-hosted MI, consistent with their formation at later stages in the crystallization of their parental melt compared to olivines. Chlorine isotopic composition ($\delta^{37}$Cl) of MI in the five Apollo basalts have weighted averages of $+12.8 \pm 2.4$‰ and $+10.1 \pm 3.2$‰ for olivine- and pyroxene-hosted MI, respectively, which are statistically indistinguishable. These isotopic compositions are also similar to those measured in apatite in these lunar basalts, with the exception of sample 14072, which is known to have a distinct petrogenetic history compared to other mare basalts. Based on our dataset, we conclude that, post-MI-entrapment, no significant Cl isotopic fractionation occurred during the crystallization and subsequent eruption of the parent magma and that Cl isotopic composition of MI and apatite primarily reflect the signature of the source region of these lunar basalts. Our findings are compatible with the hypothesis that in the majority of the cases the heavy Cl isotopic signature of the Moon was acquired during the earliest stages of LMO evolution. Interestingly, MI data from 14072 suggests that Apollo 14 lunar basalts might be an exception and may have experienced post-crystallization processes, possibly metasomatism, resulting in additional Cl isotopic fractionation recorded by apatite but not melt inclusions.

© 2019 The Author(s). Published by Elsevier B.V. This is an open access article under the CC BY license (http://creativecommons.org/licenses/by/4.0/).

## 1. Introduction

Lunar samples exhibit a wide range of measured Cl isotopic ratio (Barnes et al., 2016; Boyce et al., 2015; Potts et al., 2018; Sharp et al., 2010; Tartèse et al., 2014; Treiman et al., 2014) compared to the Earth (Bonifacie et al., 2008; Manzini et al., 2017; Sharp et al., 2013). Indeed, in case of the Moon the Cl isotopic ratio, reported as $\delta^{37}$Cl values (in per mil), ranges from $-4$ to $+18$‰ in mare basalts (Barnes et al., 2016; Boyce et al., 2015; Sharp et al., 2010), $+14$ to $+40$‰ in KREEP-rich basalts (Barnes et al., 2016; Potts et al., 2018; Sharp et al., 2010; Tartèse et al., 2014) and $+25$ to $+36$‰ in highlands materials (Barnes et al., 2016; Treiman et al., 2014), while Earth's mantle is $\leq -1.6$‰ (Bonifacie et al., 2008) and no significant Cl isotopic variations is observed among major terrestrial reservoirs (i.e. $\sim +0.1 \pm 0.4$‰; Sharp et al., 2007). Earth and the Moon show little or no variations for many isotope systems

* Corresponding author.
*E-mail address:* alice.stephant@open.ac.uk (A. Stephant).

https://doi.org/10.1016/j.epsl.2019.115715
0012-821X/© 2019 The Author(s). Published by Elsevier B.V. This is an open access article under the CC BY license (http://creativecommons.org/licenses/by/4.0/).

such as silicon (Armytage et al., 2012), oxygen (Wiechert et al., 2001; Spicuzza et al., 2007; Hallis et al., 2010; Young et al., 2016; Greenwood et al., 2018), titanium (Zhang et al., 2012) and tungsten (Kleine et al., 2005; Dauphas et al., 2014; Kruijer et al., 2015). This general feature has significant implications for the origin of the Moon (Canup, 2012; Cuk and Steward, 2012; Canup et al., 2015; Rubie et al., 2015). Interestingly, heavy isotope enrichment in lunar rocks compared to the Earth are observed for several volatile to moderately volatile elements such as zinc (Moynier et al., 2006; Paniello et al., 2012; Kato et al., 2015), rubidium (Pringle and Moynier, 2017), potassium (Wang and Jacobsen, 2016) and gallium (Kato and Moynier, 2017), arguing for a volatile loss from the Moon either during the giant impact (Paniello et al., 2012; Wang and Jacobsen, 2016) or during the LMO differentiation (Day and Moynier, 2014; Kato et al., 2015). Several hypotheses have been proposed to account for this large spread in $\delta^{37}$Cl composition in lunar samples. Sharp et al. (2010) performed the first analyses for Cl isotopes in lunar basalts and suggested that volatilization of metal chlorides (e.g. $FeCl_2$ or $ZnCl_2$) during the eruption of mare magmas was responsible for the observed Cl isotopic fractionation. This hypothesis was founded on the fact that the lowest $\delta^{37}$Cl measured in lunar samples overlapped with the terrestrial values. The heavier $\delta^{37}$Cl values relative to $\sim 0‰$ were argued to be the result of isotopic fractionation during degassing of lunar magmas upon their eruption and emplacement. This hypothesis implies that the Moon is anhydrous, as any significant presence of H in mare magmas would have resulted in the degassing of HCl instead of metal chlorides, which would not have produced the Cl isotopic fractionation observed in late crystallising phases such as apatite. Indeed, in hydrous magmatic reservoirs in terrestrial setting where degassing of HCl is predominant, loss of $^{35}$Cl is accompanied by a similar loss of $^{37}$Cl, resulting in no net isotopic fractionation (Sharp et al., 2010). However, for the Moon, this scenario goes against numerous studies arguing for a relatively wet Moon (Hauri et al., 2011; Saal et al., 2008), albeit still volatile-depleted compared to the Earth (Albarede et al., 2015).

Further studies, based on correlated analyses of H and Cl abundances and their isotopic compositions in lunar apatite (Barnes et al., 2016; Boyce et al., 2015, 2018), have challenged the hypotheses of an anhydrous Moon and the Cl isotopic fractionation by degassing during the magma emplacement stage (cf. also referred as lava-outgassing (Boyce et al., 2015)). As such, (i) the presence of OH-rich apatites (Barnes et al., 2013; McCubbin et al., 2015; Tartèse et al., 2013), (ii) the absence of negative correlation between Cl content and $\delta^{37}$Cl (Barnes et al., 2016), (iii) the absence of any correlation between $\delta$D and $\delta^{37}$Cl in lunar apatite (Boyce et al., 2015), and (iv) the abundance of Cl relative to refractory incompatible elements such as U and Th in low-Ti and KREEP-rich basalts (Boyce et al., 2018) argue against lava-outgassing as being the major control over Cl isotopic fractionation. An alternative scenario is envisaged to explain the elevated $\delta^{37}$Cl in lunar basalts, which includes mixing between 2 reservoirs: a lighter one ($\sim 0‰$), representative of mare-basalt source regions and an elevated one (i.e. 25–30‰) from urKREEP reservoir, the final product of the LMO crystallisation. The heavy Cl isotopic composition of the urKREEP reservoir is thought to have been acquired either during the incremental degassing of the LMO (Boyce et al., 2015) or by the degassing of the KREEP-rich layer exposed to vacuum of space during crust-breaching impact event(s) (Barnes et al., 2016) or in some cases, a vapor-induced metasomatism $\sim 4$ Ga ago (Potts et al., 2018; Treiman et al., 2014).

A potential shortcoming with lunar Cl measurements to date, with the exception of few bulk measurements on glasses (Sharp et al., 2010), is that they have been performed on apatite (Barnes et al., 2016; Boyce et al., 2015; Potts et al., 2018; Sharp et al., 2010; Tartèse et al., 2014). During the crystallisation of mare magmas, apatite typically forms after $> 95\%$ fractional crystallization and as such, it is not possible to confirm whether the Cl isotope fractionation occurs prior to or during the crystallization of the parent magma. In order to evaluate the possibility of isotopic fractionation during crystallization and eruption of lunar basalt, and explore other alternatives, a more pristine, early-crystallised phase should be targeted in the same samples from which apatite were analysed. Moreover, Cl abundance in parent magma can be more easily determined from melt inclusions as they provide direct measurement of the parent melt.

Silicate-hosted MI are small blebs of silicate melts trapped within phenocrysts at magmatic pressures and temperatures (Cannatelli et al., 2016; Lowenstern, 2003; Métrich et al., 2008; Roedder, 1979; Walker et al., 1976). The phenocryst host acts as a pressure vessel during eruption, keeping any primary MI isolated from subsequent degassing or crystal fractionation effects during the eruption and emplacement of a magma. The silicate-hosted MI are of particular interest as they trap magmatic liquid at the time of their host crystallization and as such, record the composition and the evolution of the magma at the time of trapping. Moreover, MI represent the only tool that can directly provide the pre-eruptive volatile (such as $H_2O$, Cl, $CO_2$, S, F) content of a magma, although diffusion (Bucholz et al., 2013; Gaetani et al., 2012; Hauri, 2002) and post-entrapment crystallization (PEC) (Danyushevsky et al., 2002; Steele-MacInnis et al., 2011) could alter the initial H budget.

There have been numerous studies investigating volatile contents in MI to infer the volatile budget of volcanic systems on the Earth (e.g. Esposito et al., 2012; Hauri, 2002), the Moon (e.g. Chen et al., 2015; Hauri et al., 2011; Saal et al., 2013; Singer et al., 2017) and Mars (e.g. Giesting et al., 2015; Usui et al., 2012). Pioneering work on lunar MI was carried out by Roedder and Weiblen (1970; 1971) who made an exhaustive list of MI petrographic characteristics. A few studies have measured the Cl contents of MI from lunar samples, including the Apollo 17 sample, 74220 (Chen et al., 2015; Hauri et al., 2011), which is a high-Ti volcanic glass produced by pyroclastic eruption, as well as in lunar basalts 10020, 12008, 12040 and 15016 (Chen et al., 2015; Ni et al., 2019). However, no data have been reported previously on Cl isotopic composition of lunar MI.

Here, for the first time, we report Cl abundance and its isotopic composition in a large selection of silicate-hosted MI from five Apollo basalts. This selection includes glassy and partially crystallized MI in both olivine and pyroxene hosts. The aim of this study is to: (i) determine the Cl abundance of the mantle source-regions of mare basalts; (ii) to track the evolution of Cl abundance and isotopic composition during the crystallization of mare magmas; and (iii) to infer process(es) influencing Cl isotopic fractionation in lunar samples.

## 2. Materials and methods

### 2.1. Samples

The selection of samples was based on several criteria. Firstly, we selected five mare basalts from four Apollo landing sites, in order to document any lateral heterogeneity for Cl in the lunar mantle as sampled by mare magmas. Indeed, it has been argued previously that lunar volatile abundances, and especially water, are associated with local heterogeneities in the lunar mantle and are not globally representative of the Moon (Albarede et al., 2015). The samples selected are 10020, which is a low-K ilmenite basalt (Kramer et al., 1977; Meyer, 2009); vesicular olivine basalts 12004 and 12040 which are low-Ti basalts; KREEP-rich olivine basalt 14072 and low-Ti vesicular olivine basalt 15016 (Meyer, 2009). Secondly, we selected these mare basalts based on their cooling

rates, in order to evaluate the effect of cooling on Cl signatures in lunar magmas. Two samples were selected from Apollo 12 collections, to investigate the evolution of volatiles during the cooling history of magmas derived from the same basaltic reservoir, as has been done previously for H isotopes (Singer et al., 2017). The more rapidly cooled samples are 10020 (3 °C/h—Beaty and Albee, 1978; Rhodes and Blanchard, 1980), 12004 (Walker et al., 1976) and 14072 while the two samples more slowly cooled are 12040 (Walker et al., 1976) and 15016 (0.6 °C/h—Tikoo et al., 2012). Finally, Cl abundances for three samples that we selected (10020, 12040 and 15016) were previously also measured in olivine-hosted MI by Chen et al. (2015); while Cl isotopic compositions and abundances have been reported for apatite in mare basalts 12040 (Boyce et al., 2015), 14072 (Potts et al., 2018) and 15016 (Barnes et al., 2019). Thus, we are able to compare and cross-check our data on Cl abundances with previous measurements while extending the database of volatiles for lunar MI. Finally, in order to monitor the evolution of Cl abundance and its isotopic composition in the lunar magma, we analysed both olivine- and pyroxene-hosted MI. Indeed, olivine- and pyroxene-hosted MI were trapped at different times during the crystallization of the parent magma and thus provide snapshots of magma composition at the instant of melt trapping. Therefore, our approach should allow us to identify any magmatic processes that would have altered the Cl content and/or $\delta^{37}$Cl in lunar samples during crystallisation.

### 2.2. Identification of melt inclusions: SEM and Raman

Olivine and pyroxene phenocrysts containing MI were identified by optical microscopy and the FEI Quanta 200 3D Dual Beam scanning electron microscope (SEM) at The Open University (OU). Samples were also analysed using a Jobin-Yvon Horiba LabRam HR Raman microprobe at the OU, with a green (514 nm) laser excitation source delivering 1 mW at the sample surface, and a 600 grooves/mm grating to provide a spectral resolution of $\sim 3$ cm$^{-1}$. The laser beam was focused through a microscope equipped with a $\times 50$ objective (N.A. 0.75), providing a spatial resolution of $\sim 1$ µm. Spectra were collected for each sample in the range of 100–4000 cm$^{-1}$. The exposure time for each spectrum was 60 s and three accumulations were obtained for each analytical spot. Peak position was calibrated daily against a silicon wafer prior to sample analyses.

### 2.3. NanoSIMS protocol

Cl abundance and its isotopic composition were measured using the Cameca NanoSIMS 50L at OU using a protocol modified after Tartèse et al. (2014) and Barnes et al. (2016). Analyses were carried out using a $Cs^+$ primary beam with a diameter of $\sim 1$ µm and an accelerating voltage of $\sim 16$ kV. A 300–500 pA primary current was rastered over the sample on areas ranging between 10 µm × 10 µm to 30 µm × 30 µm, depending on the sizes of MI. Each analysis surface area was divided into 128 × 128 pixels, with a counting time of 1 ms per pixel. The number of cycles was set at 100. Three to ten minutes of pre-sputtering was set-up before analysis on a larger area than the analysed surface to remove any contamination from the surface and establish sputter equilibrium. An electron flood gun was used for charge compensation. Secondary negative ions of $^{18}$O, $^{29}$Si, $^{35}$Cl, $^{37}$Cl and $^{27}$Al$^{16}$O were imaged by scanning ion imaging, with a MRP of 7000. Basaltic glass MD57-D9-1 (Bonifacie et al., 2008) was used for relative sensitivity factor of Cl abundance and San Carlos olivine was used for establishing background counts for Cl. Data were processed with the L'IMAGE software developed by Larry Nittler from the Carnegie Institute of Washington. The deadtime was set at 44 ns and corrected with the L'IMAGE software. Regions of interest (ROIs) were determined on each image based on the $^{27}$Al$^{16}$O/$^{18}$O and $^{35}$Cl/$^{18}$O images to locate the MI and exclude any cracks, voids or anomalously Cl-rich hotspots associated with extraneous contamination (see section 3.2). Indeed, MI are enriched in $^{27}$Al$^{16}$O compared to their nominally anhydrous host and contamination induced hotspots of $^{35}$Cl. Because the beam overlaps at boundaries between phenocryst host and MI, ROIs were defined on $^{27}$Al$^{16}$O/$^{18}$O counts plateau to make sure only MI material is taken into consideration for their $^{35}$Cl/$^{18}$O and $^{37}$Cl/$^{35}$Cl ratios. All $^{27}$Al$^{16}$O/$^{18}$O and $^{35}$Cl/$^{18}$O NanoSIMS images with defined ROIs are provided in supplementary Fig. S1.

Melt inclusion Cl abundances were calibrated using the measured $^{35}$Cl/$^{18}$O ratios and the known Cl abundances of terrestrial MORB standards SR2-DR04 and MD57-D9-1 (Bonifacie et al., 2008), as well as DR5, DR15 and DR32 (Clog, 2010). These standards were set in an indium amount. Average count rate of $^{35}$Cl for a $\sim 12$ µm × 12 µm ROI area in MD57-D9-1 was $\sim 3000$ counts per second ($50 \pm 10$ ppm). A negligible Cl background was determined using San Carlos olivine (0.04 count rate per second of $^{35}$Cl for ROI of $\sim 12$ µm × 12 µm). The slope of the calibration line was estimated using R program to be $3.08 \times 10^{-4} \pm 0.6 \times 10^{-4}$ at 95% confidence level (Fig. S2), taking into accounts analytical errors on glass standards. Uncertainties reported on Cl contents combine the $2\sigma$ analytical uncertainties associated with each individual measurement and the uncertainty associated with the calibration line. Chlorine concentrations in MI were corrected for post-entrapment crystallization (PEC), determined using the software Petrolog3 (Danyushevsky and Plechov, 2011).

For Cl isotope measurements, the instrumental mass fractionation (IMF) factor, $\alpha$, based on analyses of SR2-DR04 and MD57-D9-1 MORB glass standards is $1.008 \pm 0.003$ (2SD). The measured $^{37}$Cl/$^{35}$Cl ratios are corrected for the IMF and expressed in $\delta^{37}$Cl notation as defined in equation (1), with standard mean ocean chloride $\delta^{37}$Cl SMOC = 0‰ (Kaufman et al., 1984). Errors estimated for $\delta^{37}$Cl values take into consideration the error based on counting statistics, as well as the uncertainty associated with the IMF calculation.

$$\delta^{37}\mathrm{Cl}(‰) = \left[\left({}^{37}\mathrm{Cl}/{}^{35}\mathrm{Cl}_{\mathrm{sample}}\right)/\left({}^{37}\mathrm{Cl}/{}^{35}\mathrm{Cl}_{\mathrm{SMOC}}\right) - 1\right] \times 1000 \quad (1)$$

The Cl isotopic composition from some MI could not be precisely determined because of counting statistics (2SD on $\delta^{37}$Cl > 10‰) and are, therefore, not reported here.

Glass standards SR2-DR04 and MD57-D9-1 were both measured on each of the five days. In order to verify the accuracy and reproducibility of our analyses, we treat one of the standards as unknown and recalculate its $\delta^{37}$Cl value relative to the other standard for each of these five days using the other standard as the known one (cf. Table S2–Fig. S3). MD57-D9-1 has a Cl content of $50 \pm 10$ ppm, which is closest in abundance to that of Apollo MIs. The average for these five independent $\delta^{37}$Cl measurements for MD57-D9-1 is $-1.7 \pm 2.3$‰, while its true value is $-1.4 \pm 0.7$‰, demonstrating good reproductivity and accuracy for these measurements at low Cl abundances, providing confidence in our result at a level of $\sim \pm 2$‰. Furthermore, the Cl isotope measurements employed in this study were based upon a recent protocol developed by Barrett et al. (2019). In particular, using a standard with as little as 17 ppm Cl they reported no isotopic effects with Cl abundance down to levels comparable to those in some of the samples reported here.

**Table 1**
Cl content and $\delta^{37}$Cl values relative to SMOC and associated 2$\sigma$ errors for olivine- and pyroxene-hosted MI in 10020,31, 12004,51, 12040,44, 14072,13 and 15016,14 Apollo basalts. *Cl content (ppm) corrected from PEC. **PEC (%) is determined using Petrolog3 (Danyushevsky and Plechov, 2011). Mg# of the host mineral is also given. Isotopic compositions for MI with statistical error higher than 10‰ are not determined (*n.d.*) (cf. NanoSIMS protocol).

| Sample | Olivine–MI # | Cl (ppm) | Cl (ppm) PEC* | 2$\sigma$ | $\delta^{37}$Cl (‰) | 2$\sigma$ | Mg# host | PEC (%)** |
|---|---|---|---|---|---|---|---|---|
| **10020.31** | | | | | | | | |
| | MI 2 | 24.2 | 10.0 | 4.3 | 8.1 | 3.6 | 70.2 | 58.5 |
| | MI 12 | 6.9 | 5.2 | 1.2 | 9.3 | 9.7 | 68.6 | 24.6 |
| | MI 22A | 9.7 | 5.0 | 1.7 | 13.9 | 7.8 | 68.2 | 48.8 |
| | MI 22B | 9.2 | 4.9 | 1.7 | 6.6 | 9.0 | 69.5 | 46.7 |
| **12004.51** | | | | | | | | |
| | MI 1 | 3.4 | 1.3 | 0.6 | *n.d.* | *n.d.* | 66.0 | 63.0 |
| | MI 13 | 7.0 | 2.4 | 1.3 | 11.2 | 6.9 | 67.0 | 65.1 |
| | MI 24A | 4.7 | 1.7 | 0.8 | 13.1 | 9.3 | 70.3 | 64.7 |
| | MI 24C | 5.6 | 3.2 | 1.0 | *n.d.* | *n.d.* | 71.7 | 42.8 |
| | MI 27 | 11.0 | 4.7 | 2.0 | 9.8 | 3.9 | 67.0 | 57.6 |
| **12040.44** | | | | | | | | |
| *Glassy* | MI 4A | 8.0 | 8.0 | 1.4 | *n.d.* | *n.d.* | 50.7 | |
| | MI 4B | 6.7 | 3.7 | 1.2 | 15.9 | 5.9 | 50.7 | 44.6 |
| *Glassy* | MI 9 | 14.0 | 14.0 | 2.5 | *n.d.* | *n.d.* | 60.5 | |
| | MI 12 | 6.3 | 2.9 | 1.1 | 26.3 | 8.9 | 56.1 | 53.6 |
| | MI 16 | 8.0 | 3.5 | 1.4 | 15.1 | 5.8 | 55.6 | 55.7 |
| | MI 21A | 5.2 | 2.4 | 0.9 | *n.d.* | *n.d.* | 56.5 | 53.3 |
| | MI 21B | 35.3 | 28.2 | 6.4 | 17.1 | 3.7 | 56.5 | 20.2 |
| | MI 32 | 6.6 | 4.2 | 1.2 | *n.d.* | *n.d.* | 53.8 | 36.7 |
| **14072.13** | | | | | | | | |
| | MI 2A-a | 3.7 | 1.4 | 0.7 | *n.d.* | *n.d.* | 73.2 | 62.4 |
| | MI 2A-d | 3.6 | 1.4 | 0.7 | *n.d.* | *n.d.* | 73.2 | 62.4 |
| | MI 2B | 5.3 | 3.2 | 1.0 | 10.1 | 6.9 | 70.0 | 39.0 |
| | MI 15 | 2.9 | 1.3 | 0.5 | *n.d.* | *n.d.* | 74.3 | 55.1 |
| | MI 39 | 6.4 | 3.2 | 1.2 | 8.3 | 9.9 | 56.4 | 50.0 |
| **15016.14** | | | | | | | | |
| | MI 4 | 8.4 | 4.8 | 1.5 | 15.0 | 5.3 | 42.6 | 42.6 |
| *Glassy* | MI 8 | 13.6 | 12.7 | 2.5 | 13.2 | 6.4 | 34.4 | 7.0 |
| | MI 23 | 6.3 | 5.1 | 1.1 | *n.d.* | *n.d.* | 54.0 | 19.3 |
| *Glassy* | MI 26 | 4.6 | 4.6 | 0.8 | 13.4 | 9.4 | 23.6 | |
| Sample | Pyroxene–MI # | Cl (ppm) | Cl (ppm) PEC* | 2$\sigma$ | $\delta^{37}$Cl (‰) | 2$\sigma$ | Mg# host | PEC (%)** |
| **10020.31** | | | | | | | | |
| | MI 20A | 16.1 | 7.8 | 2.9 | 13.0 | 6.9 | 64.4 | 51.5 |
| | MI 20B | 13.1 | 6.5 | 2.4 | *n.d.* | *n.d.* | 64.4 | 50.3 |
| **12004.51** | | | | | | | | |
| | MI 9 | 2.9 | 1.3 | 0.5 | *n.d.* | *n.d.* | 60.0 | 54.5 |
| | MI 16 | 3.6 | 1.6 | 0.7 | *n.d.* | *n.d.* | 63.4 | 55.4 |
| **12040.44** | | | | | | | | |
| | MI 24A | 34.3 | 9.7 | 6.20 | 33.4 | 4.2 | 72.4 | 71.8 |
| | MI 24B | 5.5 | 1.7 | 1.00 | 9.7 | 9.8 | 69.9 | 68.4 |
| | MI 24D | 59.0 | 27.1 | 10.60 | 11.9 | 5.5 | 69.9 | 54.0 |
| **14072.13** | | | | | | | | |
| | MI 26 | 13.5 | 7.2 | 2.4 | *n.d.* | *n.d.* | 66.5 | 46.5 |
| **15016.14** | | | | | | | | |
| | MI 1 | 78.4 | 31.3 | 14.1 | 11.5 | 4.8 | 66.5 | 60.1 |
| | MI 16 | 14.4 | 8.0 | 2.6 | 15.6 | 7.8 | 26.9 | 44.7 |
| | MI 37 | 59.8 | 28.9 | 10.8 | 4.5 | 4.6 | 51.4 | 51.6 |

## 3. Results

### 3.1. Petrographic context of melt inclusions

A total of 25 MI in olivines, among which 4 appear glassy (less than 10% PEC), and 11 MI in pyroxenes, were identified from the 5 Apollo thin sections. PEC ranges from 7% to 65% in olivine-hosted MI, with an average of 46% while in pyroxene-hosted MI, PEC ranges from 37% to 72% with an average of 54% (Table 1). Selected back scattered electron (BSE) images, demonstrating the diversity of analysed MI, are shown in Fig. 1, while BSE images of all MI analysed in study are provided in supplementary Fig. S1. For olivine-hosted MI, we found 4 glassy type in thin sections 12040,44 and 15016,14. Indeed, glassy MI are extremely rare in lunar samples and are particularly small, i.e. less than $\sim$ 5 µm in diameter, compared to partially crystalline MI (Roedder and Weiblen, 1970). Interestingly, the two Apollo samples where we found glassy MI are the two slowly cooled basalts compared to the three others lunar basalts investigated in this study. Fig. 1A shows a BSE image of two MI in a single olivine phenocryst in 12040,44 (MI#4a and #4b). MI#4a-12040 is a typical small glassy MI, less than $\sim$ 5 µm in diameter, with a bubble. Bubbles in lunar MI are most probably a result of post-entrapment exsolution from the melt during cooling and as such are denominated as shrinkage bubble. MI#4b-12040 is a partially crystallized MI with a typical single opaque phase daughter mineral which is ilmenite in this case (e.g. Fig. 1A–B–C) (Roedder and Weiblen, 1970). The second most common daughter mineral is troilite which occurs as spherical opaque particles (e.g. Fig. 1B), followed by plagioclase and pyroxene. Glassy MI are extremely small compared to partially crystallized MI, as large inclusions crystallize faster than the small ones (Roedder, 1984). Indeed, the largest crystallized MI, i.e. MI#2-14072, has a dimension of $\sim$ 120 µm $\times$ 80 µm (cf. Fig. 1B). Some olivines exhibit an assemblage of MI as shown previously for MI#4a and #4b from 12040 basalt. The biggest MI Assemblage (MIA), was found in 12004,51 (Fig. 1C). Melt inclusions forming an assemblage are trapped approximately at the same time, same temperature and pressure and come from a melt

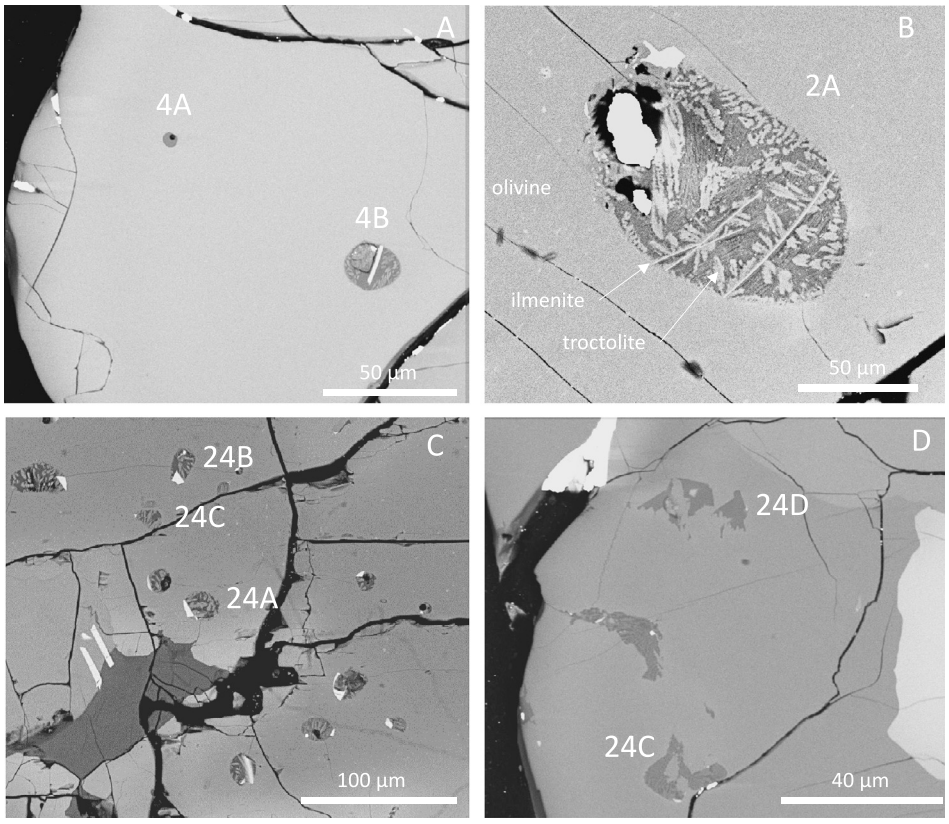


**Fig. 1.** BSE images of melt inclusions in olivines (A–B–C) and pyroxenes (D) in the studied Apollo thin sections. A—Glassy MI #4a and partially crystallized MI #4b in 12040,44 in an olivine crystal. The glassy 4a is extremely small ($\sim$ 5 µm) compared to partially crystallized MI. B—Large $\sim$ 120 µm $\times$ 80 µm partially crystallized MI#2 in 14072,13. This olivine-hosted MI is the largest one analysed. C—Assemblage of olivine-hosted MI (#24) in 12004,51. D—Assemblage of pyroxenes MI in 12040,44. MI#24b is partially crystallized while MI#24d is entirely glassy. They have an irregular outline compared to olivine-hosted MI that are typically oval in shape.

with the same composition. These MIA are a good way to compare volatile content and isotopic composition of MI in a single phenocryst, and look for any variation revealing certain magmatic physical–chemical process (Cannatelli et al., 2016). As such, MIA are a recommended target for accurate MI studies. A total of 5 MIA were analysed in olivines. All of the olivine-hosted MI have round to oval shapes, irrespective of whether they are glassy or partially crystallized. Only a few olivine-hosted MI studied here presented a single shrinkage bubble at their polished surface (e.g. Fig. 1A). Assuming these observations to be representative of lunar case, the presence of single shrinkage bubble, or no bubble in MI is consistent with relatively volatile-depleted nature of lunar magmas compared to terrestrial ones (Albarede et al., 2015).

Pyroxene-hosted MI are different from olivine-hosted MI in the sense that they commonly have an irregular shape (e.g. Frezzotti, 2001; Kent and Elliott, 2002). Fig. 1D shows a MIA in a pyroxene phenocryst in 12040,44. Because of their non-usual shape, pyroxene-hosted MI are more difficult to identify than olivine-hosted MI. We used Raman spectra to confirm location of glassy areas in these types of MI. Fig. 2 is an example of Raman spectra obtained for a pyroxene-hosted MI, in comparison with its host's (pyroxene) spectra. The Raman spectra for the MI#1 in 15016,14 isn't completely featureless but we can still observe a significant difference between the MI and its host pyroxene spectrum. This is due to the high PEC of 60% estimated for this MI.

### 3.2. NanoSIMS scanning ion imaging

The NanoSIMS imaging mode was chosen instead of dynamic analysis mode based upon several lines of reasoning, as illustrated in Fig. 3 (all $^{27}Al^{16}O/^{18}O$ and $^{35}Cl/^{18}O$ NanoSIMS images are provided in supplementary Fig. S1). Firstly, the $^{27}Al^{16}O/^{18}O$ ratio image allowed us to identify the MI location in the host phenocryst. Indeed, most MI are small, especially the glassy ones in olivine, which have a diameter of $< 5$ µm and therefore it is challenging to perform a spot analysis of the MI only. NanoSIMS imaging, with the relatively small probe diameter used in this study, allowed integration of signal from only the MI during data processing (see methods). As an example, BSE and NanoSIMS image of the glassy MI#26 from 15016,14 are shown in Fig. 3A, as well as the pyroxene-hosted MI#24A from 12040.44 sample in Fig. 3B. A region of interest (ROI) was then defined (white dashed lines on Fig. 3), surrounding solely the MI. Note the low counts of $^{35}Cl/^{18}O$ associated with this glassy olivine-hosted MI (Fig. 3A—corresponding to $4.6 \pm 0.8$ ppm Cl). The second line of reasoning was that bubble, cracks and Cl-rich phases could be observed on $^{35}Cl/^{18}O$ images as they induced hotspots in Cl counts. Fig. 3C shows BSE and NanoSIMS images of MI#4a from 12040,44, which is a glassy MI containing a shrinkage bubble. Clearly, a hotspot in $^{35}Cl/^{18}O$ counts defined the bubble in the MI, most likely contamination introduced during polishing. The $^{35}Cl/^{18}O$ counts are much higher compared to the glassy part of the MI, as well as the glassy MI#26 from 15016,14 (Fig. 3A). The same applied to cracks (cf. Fig. 3D). Definition of ROIs were made in order to exclude contributions from these features. Finally, $^{27}Al^{16}O/^{18}O$ maps of partially crystallized MI allowed us to distinguish melt-only vs. crystallized regions. For instance, MI#39 from 14072,13 is a partially crystallized MI, with the melt-area located mostly in its centre (cf. Fig. 3C). The $^{27}Al^{16}O/^{18}O$ NanoSIMS image of MI#39-14072 exhibits higher $^{27}Al^{16}O/^{18}O$ ratios in the melt areas compared to the areas containing daughter minerals. Here again, ROI is defined accordingly. Using NanoSIMS imaging instead of spot analyses provided extra reassurance that almost

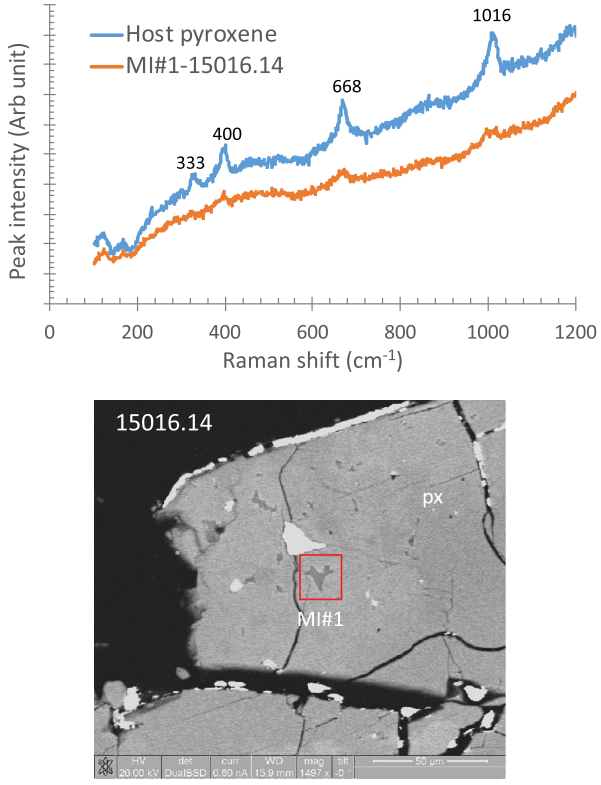


**Fig. 2.** Raw Raman spectrum obtained for MI#1 in 15016,14, as well as spectrum for the host pyroxene. Y-axis in is arbitrary units. Peak Raman shift ($cm^{-1}$) are written for the host pyroxene. (For interpretation of the colours in the figure(s), the reader is referred to the web version of this article.)

exclusively the melt portions of MI were taken into consideration for the determination of their Cl abundance as well as their $\delta^{37}$Cl value. Table 1 lists all the Cl data (abundance and isotopic composition) collected on MI in this study (All raw data are available in supplementary Table S1).

### 3.3. Effects of daughter minerals in MI on chlorine systematics

Glassy MI in lunar samples are rare compared to partially crystallized MI in olivines. Chlorine is a moderately incompatible element and remains in the residual melt phase when daughter minerals crystallize. As such, the measured Cl concentration of a MI is higher than its initial Cl content, which can be calculated using its percentage of PEC (Danyushevsky and Plechov, 2011; Hauri et al., 2011). Similar to what has been previously discussed for hydrogen isotopic measurements (Riciputi and Greenwood, 1998; Singer et al., 2017), analyses of mixed matrix in partially crystallized MI could be used to infer Cl isotopic composition of the parent melt, as the chlorine will be sited preferentially only in the glass phase. Moreover, most of the daughter crystals were already excluded by processing of NanoSIMS images (cf. previous subsection). However, in order to dismiss fully the role of MI crystallization on the measured $\delta^{37}$Cl values, we compare the $\delta^{37}$Cl composition with the percentage of post-entrapment crystallization (Fig. 4). No obvious trend appears on the $\delta^{37}$Cl (‰) vs. PEC (%) plot. Hence, no significant differences are observed for $\delta^{37}$Cl values in lunar olivine- and pyroxene-hosted MI, as a function of their degree of crystallization. Thereby, the PEC corrected Cl concentration and the measured Cl isotopic composition in partially crystallized MI can be considered as representative of values measured from glassy MI in olivines.

### 3.4. Results from olivine-hosted melt inclusions

Twenty five MI hosted in olivine were analysed from 5 Apollo basalts (Table 1). The measured Cl content ranges from $2.9 \pm 0.5$ ppm to $35.3 \pm 6.4$ ppm. Chlorine concentrations corrected for post-entrapment crystallization are 7 to 65% lower than the measured concentrations and range from $1.3 \pm 0.5$ ppm to $28.2 \pm 6.4$ ppm Cl, with twenty one measurements below 5 ppm. Corrected values are presented in Fig. 5A. On account of its large size, two separate measurements were made from a single MI (MI#2A-14072), which allowed us to test any intra-phase variation in Cl abundances (and bring the total number of analyse to 26 for olivines). As such, MI#2A-14072 show extremely good reproducibility on Cl content in a single MI, as the two measurements are similar ($1.4 \pm 0.7$ ppm in both analyses). All of the MI from individual samples appear to show broadly consistent results, although several of the samples have one measurement that is considerably higher than the rest. This may reflect indigenous heterogeneity within the sample, but in all cases most likely reflects incomplete exclusion of chlorine contamination during data processing and therefore the results from 5 measurements should be treated with caution. The concentration averages for each sample are $6.3 \pm 2.5$ ppm for 10020, $2.6 \pm 1.4$ ppm for 12004, $5.5 \pm 4.1$ ppm for 12040 (excluding 28.2 ppm outlier), $2.1 \pm 1.0$ ppm for 14072 and $6.8 \pm 3.9$ ppm for 15016. This dataset does not reveal any significant variation in Cl abundances in olivine-hosted MI among the 5 different Apollo lunar basalts. The concentration average for MI of these 5 Apollo samples is 5.5 ppm ($n = 26$). Based on the 20 MI showing a narrow range below 5 ppm (i.e. excluding the five data points at higher concentrations which might be due to contamination), the average Cl content is $3.3 \pm 1.4$ ppm (1SD, $n = 21$).

In terms of $\delta^{37}$Cl values, olivine-hosted MI in the 5 Apollo samples range from $+6.6 \pm 9.0$‰ to $+26.3 \pm 8.9$‰ (Fig. 5A). Because of the limitation posed by counting statistics for very low Cl content in olivine-hosted MI, the $\delta^{37}$Cl values are associated with relatively large uncertainties, albeit the total variation is still well within the range of Cl isotope composition recorded in lunar apatite. The weighted average for $\delta^{37}$Cl is $+8.9 \pm 3.2$‰ in 10020, $+10.5 \pm 2.3$‰ in 12004, $+17.3 \pm 5.4$‰ in 12040, $+9.5 \pm 1.8$‰ in 14072, and $+14.1 \pm 1.2$‰ in 15016. As such, even though the $2\sigma$ error associated with each analysis are relatively large because of the low counting statistics of Cl-poor MIs (cf. Table 1), the $2\sigma$ error from the weighted average of each sample is remarkably low, showing a good reproducibility of $\delta^{37}$Cl measurements of various olivine-hosted MIs in each of the five samples. This good reproducibility among each of $\delta^{37}$Cl gives confidence in the accuracy of the obtained results at low Cl concentration. It is remarkable that 5 Apollo samples, while coming from 4 different geographical locations on the Moon and having different bulk-compositions, do not exhibit any significant variations among their Cl contents and $\delta^{37}$Cl values. This is also reflected in the weighted average of $\delta^{37}$Cl in these olivine-hosted MI at $12.8 \pm 2.4$‰ ($n = 16$, 2SD).

Five olivine MIA where analysed in 10020,31, 12004,51, 12040,44 (two MIA) and 14072,13 (e.g. Fig. 1C). For every olivine MIA, the range of Cl content is extremely similar, except for MI#21A and MI#21B from 12040 which have extreme values of $2.4 \pm 0.9$ ppm for #21A and $28.2 \pm 6.4$ ppm for #21B. In terms of $\delta^{37}$Cl values, MI in one olivine of 10020,31 recorded the same $\delta^{37}$Cl values within the associated errors: MIA #22 is $+13.9 \pm 7.8$‰ and $6.6 \pm 9.0$‰.

### 3.5. Results from pyroxene-hosted melt inclusions

Pyroxenes in the studied samples can be separated in to two groups: those from the slowly cooled basalts, i.e. 12040 and 15016;

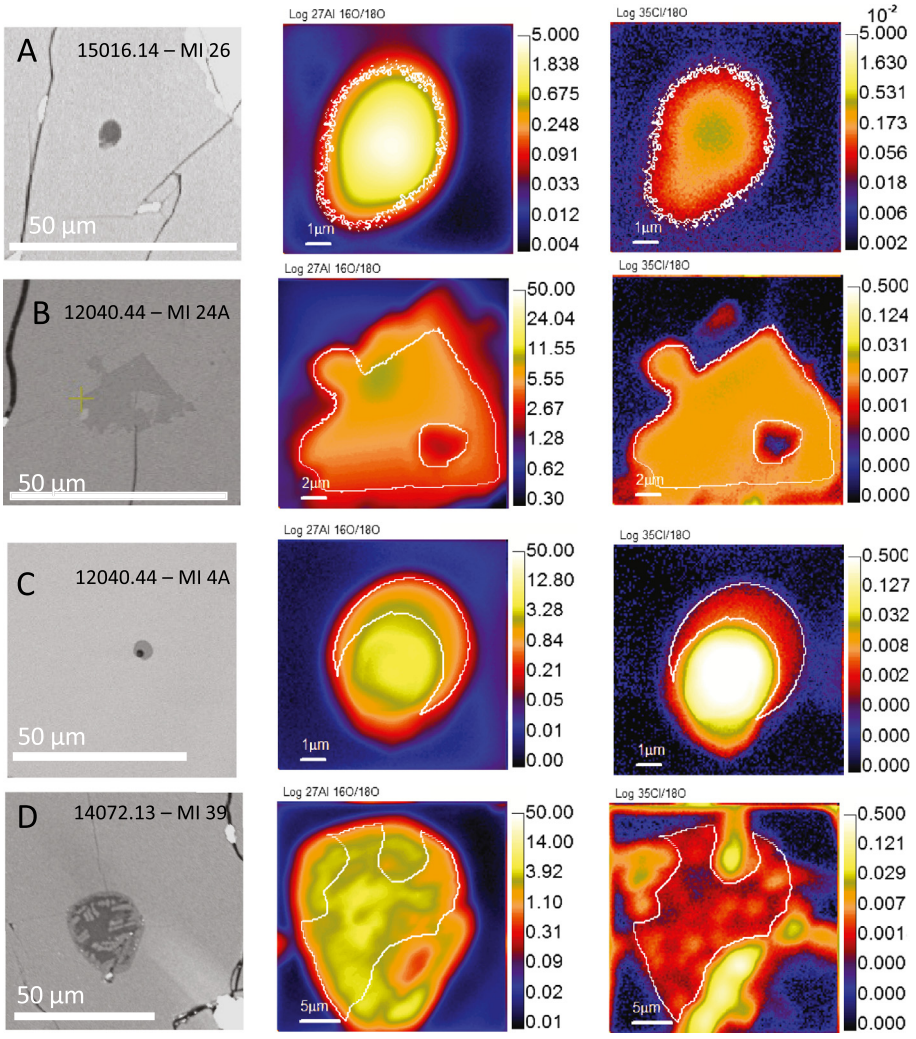


**Fig. 3.** BSE, $^{27}Al^{16}O/^{18}O$ and $^{35}Cl/^{18}O$ NanoSIMS images of four different MI. $^{27}Al^{16}O/^{18}O$ is used to identify the MI while $^{35}Cl/^{18}O$ shows large enrichment in cracks and bubbles. ROIs are outlined by white dashed lines using LIMAGE software and take into consideration only melt area in the MI defined by $^{27}Al^{16}O/^{18}O$ ratio and removal of cracks and bubbles associated with $^{35}Cl/^{18}O$ enrichment due to contamination (see text for explanation). A—Olivine-hosted glassy MI in 15016,14 (#26). The $^{35}Cl$ count associated with this MI is very low. B—Pyroxene-hosted MI in 12040,44 (#24A). C—Olivine-hosted glassy MI in 12040,44 (#4A) containing a bubble. D—Partially crystallized MI in 14072,14 (#39). Here the $^{27}Al^{16}O/^{18}O$ ratio is higher in melt area compared to areas containing daughter minerals. Also, the presence of a crack is exhibited by enrichment in $^{35}Cl/^{18}O$.

and those from more rapidly cooled basalts, i.e. 10020, 12004 and 14072. The measured Cl content ranges from $2.9 \pm 0.5$ ppm to $78.4 \pm 14.1$ ppm. Chlorine concentrations corrected for post-entrapment crystallization are 37 to 72% lower than the measured concentrations. Cl concentration corrected for PEC and its $\delta^{37}Cl$ in pyroxene-hosted MI are plotted in Fig. 5B. MI from relatively rapidly cooled basalts display Cl contents ranging from $1.3 \pm 0.5$ ppm to $7.8 \pm 2.9$ ppm. Pyroxene-hosted MI from slowly cooled basalts have a much wider range from $1.7 \pm 1.0$ ppm to $31.3 \pm 14.1$ ppm. Pyroxene-hosted MI from slowly cooled basalts, 12040 and 15016 are in general enriched in Cl compared to olivine-hosted MI and pyroxene-hosted MI in rapidly cooled basalts, presumably related to a later-stage entrapment of the MI in their host.

One pyroxene-hosted MIA was found in 12040,44 (#24). Interestingly, the three MI present display some variation in both Cl abundance and its isotopic composition. While the Cl abundance variation can be explained by difference in the time of entrapment, the heterogeneity in the Cl isotopic composition is more difficult to reconcile. In fact, MI#24B and MI#24C have similar $\delta^{37}Cl$ within errors ($9.7 \pm 9.8$‰ and $11.9 \pm 5.5$‰, respectively), but MI#24A has a $\delta^{37}Cl$ value of $+33.4 \pm 4.2$‰, which is highest value measured among all MI analysed in this study. Interestingly, one olivine-hosted MI in 12040 also exhibit a higher $\delta^{37}Cl$ of $+26.3 \pm 8.9$‰. At present it is difficult to interpret the significance of this isolated data point which is distinct from all other data points for $\delta^{37}Cl$, determined in MI from 16 olivine and 7 pyroxene hosts and, therefore, this anomalous data point of $+33.4 \pm 4.2$‰ is excluded from further discussion.

While pyroxene-hosted MI exhibit different Cl concentration as a function of the cooling rate of their parent melts, no variation is observed for their $\delta^{37}Cl$ values. Indeed, one pyroxene-hosted MI from rapidly cooled basalt 10020 has a value of $+13.0 \pm 6.9$‰ while those from slowly cooled samples 12040 and 15016 range from $+4.5 \pm 4.6$‰ to $+15.6 \pm 7.8$‰. The range of values is similar to $\delta^{37}Cl$ measured in olivine-hosted MI. The weighted average value for $\delta^{37}Cl$ for all pyroxene-hosted MI analysed in this study is $+10.1 \pm 3.2$‰ ($n = 6$; 2SD).

## 4. Discussion

### 4.1. Chlorine concentration in olivine-hosted MI

Previous works on lunar olivine-hosted MI have reported a range of 1.5 ppm to 3.9 ppm of Cl in 74220 orange glasses (Hauri

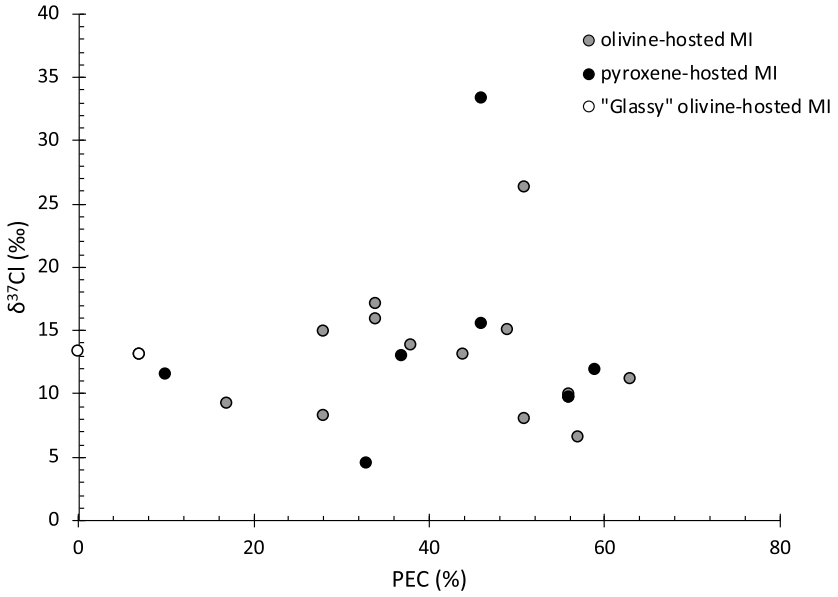


**Fig. 4.** Measured $\delta^{37}$Cl (‰) vs PEC (%) for olivine-hosted (grey), pyroxene-hosted (black) and "glassy" olivine-hosted (white) MI. No significant differences are observed as a function of the PEC of MI. The degree of post-entrapment crystallisation do not fractionate the Cl isotopic composition of the MI.

et al., 2011; Chen et al., 2015; Ni et al., 2019), 0.1 ppm to 11.0 ppm of Cl in 10020, 12008, 12040 and 15016 lunar basalts (Chen et al., 2015; Ni et al., 2019). As such, our average of $3.3 \pm 1.4$ ppm (1SD, $n = 24$) for olivine-hosted MI is in good agreement with previous measurements on Apollo 11, 12, and 15 lunar basalts. From our olivine-hosted MI results, we estimated a range of 0.1–1.4 ppm of Cl for the lunar mantle (for 5% to 30% partial melting), which is similar to the estimate of 0.14–0.83 ppm (Hauri et al., 2011), 0.4 ppm (Sharp et al., 2010; Ni et al., 2019), 0.3 to 0.6 ppm (Boyce et al., 2018), and towards the lower range of previously estimated range by McCubbin et al. (2015) of 0.26 to 2.9 ppm. These estimates are lower than the range of Cl concentration estimated for the Earth's mantle, which ranges from 0.9 ppm (Saal et al., 2002) to 35 ppm (Jambon et al., 1995), with an average value of $\sim$ 11 ppm Cl (Sharp and Draper, 2013 and ref. therein). As such, this implies that the Moon's interior is depleted in Cl by an order of magnitude compared to that of the Earth's mantle.

### 4.2. Pyroxene-hosted vs. olivine-hosted MI

Pyroxene-hosted MI from lunar basalts show different Cl contents than olivine-hosted MI. As such, Cl concentration reflects the time of MI trapping in their host mineral, as a result of Cl incompatibility in the major silicate minerals crystallizing from basaltic melts (Webster et al., 2009). In other words, pyroxene-hosted MI, principally in slowly cooled basalts, with higher Cl contents formed later than other MI with lower Cl contents. This allows us to follow the evolution of the volatile content during the crystallization of the parent magma, and look for magmatic processes that can fractionate the Cl isotopic composition on the Moon. Indeed, the result of slow cooling of crystallized MI can induce H diffusion (Bucholz et al., 2013; Gaetani et al., 2012; Hauri, 2002) and post-entrapment crystallization (Danyushevsky et al., 2002; Steele-MacInnis et al., 2011) through magma evolution and eruption. However, Cl concentration has been shown not to be significantly affected by loss through olivine diffusion in terrestrial MI (Le Voyer et al., 2014; Newcombe et al., 2014). Any significant influence of diffusion of Cl, post-entrapment modification of Cl isotopic composition in the MI as well as isotopic fractionation altering the Cl composition during the crystallization, pre- or post-entrapment, would result in either (i) a negative Cl-$\delta^{37}$Cl trend defined by olivine-hosted MI or pyroxene-hosted MI in a single sample, (ii) a heavier isotopic value for later trapped MI (pyroxene-hosted) compared to earlier trapped MI (olivine-hosted), again in a single sample. These trends and variations are not observed in any of the five samples, and instead similar values are observed among each sample, considering both their olivine- and pyroxene-hosted MI. This level of reproducibility argues against any influence of secondary processes altering the Cl concentration and isotopic values of lunar MIs. Finally, all the pyroxene-hosted MI from the five samples, independent of the cooling rate of their parent basalt, as well as all olivine-hosted MI, whatever their degree of crystallization, show the same range of $\delta^{37}$Cl (cf. Fig. 5), i.e. $+12.8 \pm 2.4$‰ and $+10.1 \pm 3.2$‰ on average. Considering that MI measured here come from 4 Apollo landing sites, this enrichment of $^{37}$Cl relative to $^{35}$Cl must be widespread across basaltic lunar reservoirs, at least on the near side of the Moon.

### 4.3. Comparison between $\delta^{37}$Cl of silicate-hosted melt inclusions and apatite in lunar basalts

#### 4.3.1. The special case of Apollo 14 high-Al basalts

Apatite in 14072 lunar basalt were analysed previously for Cl abundance and its isotopic composition (Potts et al., 2018). Apollo 14 basalts seem to record a complex petrogenetic history for Cl compared to other mare basalts. Indeed, apatite from 14072 show a range of $+16.3 \pm 2.9$‰ to $+40.0 \pm 2.9$‰ in $\delta^{37}$Cl (Potts et al., 2018), while in this study, the measured values in silicate-hosted MI are $+8.3 \pm 9.9$‰ and $+10.1 \pm 6.9$‰. As such, 14072 apatite are enriched in $^{37}$Cl compared to the initial isotopic composition of the parent magma recorded by both olivine-hosted and pyroxene-hosted MI. This feature is not observed in any other lunar basalt from Apollo 11, 12 or 15 and seems an inherent characteristic of Apollo 14 high-Al basalts. Potts et al. (2018) suggested that additional post-crystallization processes modified $\delta^{37}$Cl of apatite in Apollo 14 high-Al basalts compared to other lunar basalts. They argued that elevated $\delta^{37}$Cl in Apollo 14 high-Al basalt apatite wasn't related to urKREEP incorporation (Potts et al., 2018), in contrast to other lunar basalts, mainly low-Ti and KREEP-rich basalts (Barnes et al., 2016; Boyce et al., 2015), as their apatites are more scattered around the correlation between REE concentrations and Cl isotopic composition defined by low-Ti basalts, KREEP-rich

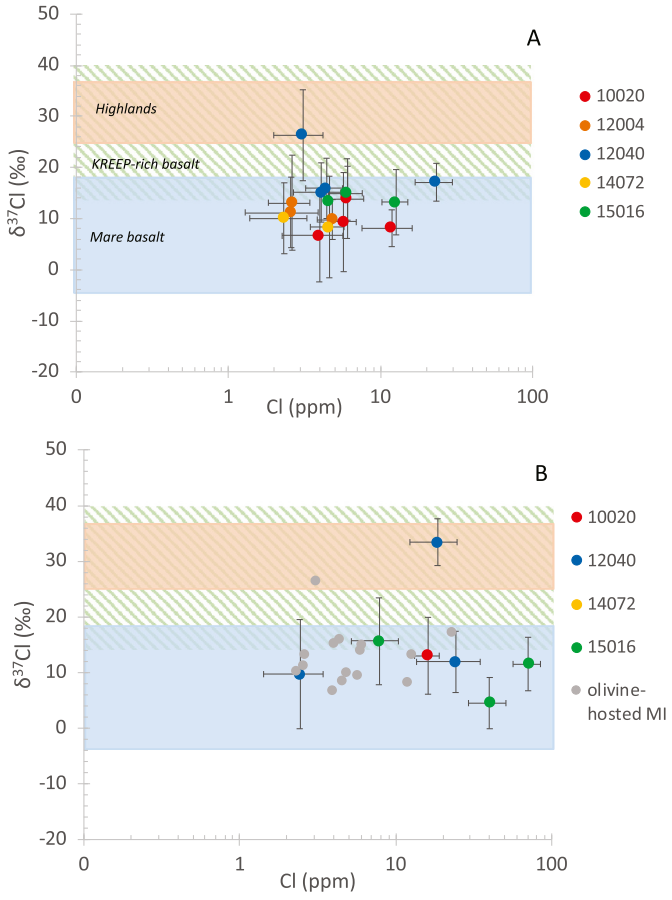


**Fig. 5.** $\delta^{37}$Cl (‰) vs Cl (ppm) for olivine-hosted MI (top-A) and pyroxene-hosted MI (bottom-B) in 10020,31, 12004,51, 12040,44, 14072,13 and 15016,14 mare basalts. The blue band corresponds to mare basalt apatite $\delta^{37}$Cl, the orange band corresponds to highlands apatite $\delta^{37}$Cl and the dashed green band stands from KREEP basalt apatite $\delta^{37}$Cl from the literature (Sharp et al., 2010; Treiman et al., 2014; Boyce et al., 2015; Barnes et al., 2016; Potts et al., 2018). In graph B, olivine-hosted MI are shown in grey circle for comparison. Pyroxene-hosted MI from rapidly cooled samples (circles) share similar Cl abundances than olivine-hosted MI while pyroxene-hosted MI from slowly cooled samples (squares) are enriched in Cl. (For interpretation of the colours in the figure(s), the reader is referred to the web version of this article.)

basalts and highland material apatites (Barnes et al., 2016) (see next subsection—Fig. 6). Nevertheless, the variability of $\delta^{37}$Cl values measured in Apollo 14 apatite has to be explained. Although sub-solidus thermal metamorphism (Taylor et al., 2004) is suggested as a possibility for modification of isotopic composition of the sample 14072, Potts et al. (2018) hypothesized that a volatile-rich vapor enriched in $^{37}$Cl interacted, in variable degrees, with the late-stage Apollo 14 basaltic and impact melts similar to the process invoked by Treiman et al. (2014) for lunar granulite 79215. On account of their encapsulation in early-formed phases, MI would be less affected than apatite by this metasomatism and, therefore, would be expected to record the initial $\delta^{37}$Cl prior to any post-crystallization modifications. Indeed, $\delta^{37}$Cl values measured in Apollo 14072 MI are in good agreement with the hypothesis of Potts et al. (2018).

#### 4.3.2. Mare basalt apatites

In apatite from mare basalts, the $\delta^{37}$Cl values range from $-4$‰ to $+18$‰ (Barnes et al., 2016; Boyce et al., 2015; Sharp et al., 2010). This range of values is similar to most measurements made in olivine- and pyroxene-hosted MI, as 34 out of 36 MI have $\delta^{37}$Cl between $+4.5 \pm 4.6$ to $+17.1 \pm 3.7$‰. A closer comparison can be done on the low-Ti basalt 12040 as its apatite have been previously measured for Cl abundance and its isotopic composition (Boyce et al., 2015). 12040 lunar basalt apatite show a range of $\delta^{37}$Cl values from $+13 \pm 3$‰ to $+17 \pm 3$‰. The six olivine- and pyroxene-hosted MI from 12040,44 analysed in this study yield a weighted average value for $\delta^{37}$Cl of $+15.9 \pm 4.7$‰ (2SD), with values ranging from $+9.7 \pm 9.8$ to $+26.3 \pm 8.9$‰. As such, apatite and silicate-hosted MI from 12040 have $\delta^{37}$Cl within the same range of values (statistical t-test p-value $= 0.6$, $\alpha = 0.05$). Similar observation can be made for low-Ti basalt 15016 in which apatite (Barnes et al., 2019) and silicate-hosted MI both have weighted average at $\sim$ 12–14‰.

Overall, $\delta^{37}$Cl of MI in both olivine and pyroxene hosts, as well as, that of apatite, from lunar mare basalts are similar, while the Cl content in the analysed phase increases in proportion to its relative time of crystallization. These results confirm that there is no Cl isotopic fractionation associated with crystallization or any other magmatic processes that would result in a preferential loss of the lighter Cl isotope, as was first suggested by Sharp et al. (2010). As such, it appears more likely that the primary magma of lunar basalts was already enriched in $^{37}$Cl relative to $^{35}$Cl, an inherent signature of lunar mantle source-regions, and that these signatures weren't altered in any significant manner during crystallization and eruption of the magma. However, an exception seems to occur for Apollo 14 basalts as highlighted above.

### 4.4. Implications for the origin of the lunar chlorine isotope fractionation compared to Earth

Our results show that lunar silicate-hosted MI have similar Cl isotopic composition than lunar apatite (with the exception of Apollo 14). As such, no fractionation of Cl isotopes occurred during the crystallization (i.e. between the early formed MI and the late formed apatite) of most basaltic parent magmas on the Moon. This is in agreement with models proposed by Boyce et al. (2015), Barnes et al. (2016) and Potts et al. (2018) arguing for an early fractionation of Cl in the Moon. Indeed, Boyce et al. (2015) suggested an early degassing of $^{35}$Cl from the molten LMO, resulting in a $\delta^{37}$Cl-rich urKREEP residual reservoir; while Barnes et al. (2016) suggested that this degassing occurred directly of the KREEP-rich layer exposed to the surface by crust-breaching impact events. Both hypotheses lead to the same result: the range of $\delta^{37}$Cl lunar values is explained by a mixing of this "degassed" $\delta^{37}$Cl-rich KREEP reservoir with $\delta^{37}$Cl-poor or isotopically lighter mare basalt reservoirs (i.e. with an isotopic composition closer to $\sim 0$‰; more comparable to the Earth's Cl isotopic composition (Bonifacie et al., 2008) than the extreme $\delta^{37}$Cl values found in the lunar materials). The main argument to support both of these theories is that a positive correlation is observed between bulk-rock REE contents (i.e. La/Lu, La/Sm) and Th contents with Cl isotopic composition of apatite in low-Ti and KREEP-rich basalts (cf. Fig. 6), highlighting that incorporation of KREEP material is causing an increase of $\delta^{37}$Cl value (Barnes et al., 2016; Boyce et al., 2015, 2018).

The $\delta^{37}$Cl of MI are plotted against bulk-rock La/Sm (normalized to CI chondrite) in Fig. 6, together with the available literature data (Boyce et al., 2015 and Barnes et al., 2016; Potts et al., 2018). At first order, low-K basalt 10020 and low-Ti basalts 12004, 12040, 15016 MI covers the same range of $\delta^{37}$Cl than low-Ti apatite (Barnes et al., 2016; Boyce et al., 2015), and as such, follow the same trend defined by apatites. Hence, our results support the mixing hypothesis of two reservoirs to account for the variety of $\delta^{37}$Cl measured in low-Ti and KREEP-rich lunar samples (Barnes et al., 2016; Boyce et al., 2015), and show that this mixing is prior to MI entrapment in olivine and pyroxene phenocrysts. However, some discrepancies appear. First, the average $\delta^{37}$Cl of the four Apollo basalts (excluding the Apollo 14 high-Al basalt—see before) slightly deviate from the correlation trend, especially

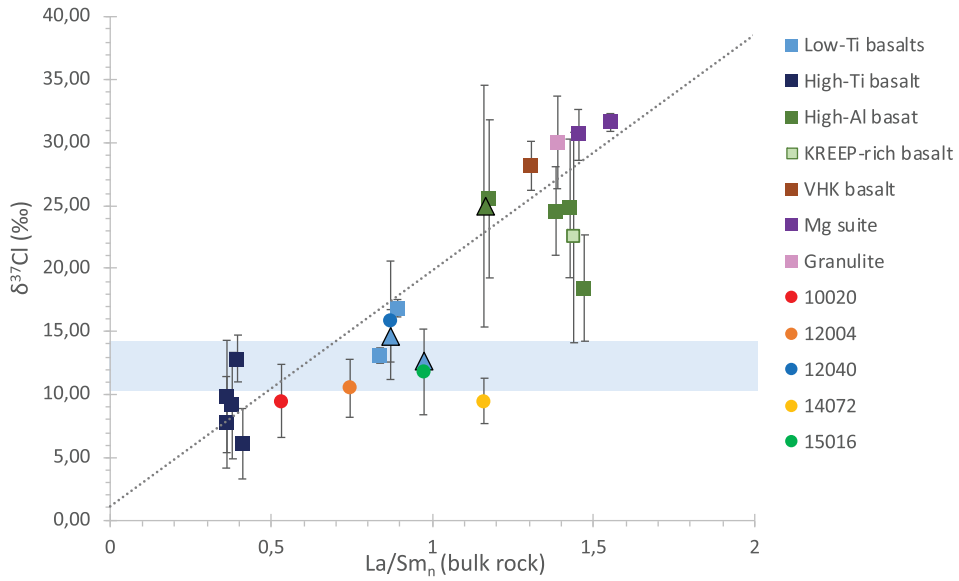


**Fig. 6.** $\delta^{37}$Cl of lunar apatites and silicate-hosted melt inclusions compared to carbonaceous chondrite-normalised La/Sm bulk-rock ratios (normalised ('*n*') using La/Sm ratios of carbonaceous chondrites given by Anders and Grevesse (1989), modified after Barnes et al. (2016). All Cl-isotope values are the average $\delta^{37}$Cl values for each sample and the uncertainties represent the standard deviation. For MI, the average represent data compiled from both olivine and pyroxene hosts. The blue area represents the average and 2 standard deviations of all olivine- and pyroxene-hosted MI measured in this study, i.e. $12.6 \pm 1.9$‰ ($n = 22$, 2SD). The dashed grey line is the correlation estimated from Barnes et al. (2016). The Cl isotope data for lunar apatites in 12040, 15016 and 14072 (triangles) are from Boyce et al. (2015), Barnes et al. (2016), Potts et al. (2018) and Barnes et al. (2019), respectively.

for 12004 and 15016. Secondly, it is remarkable that these five Apollo samples, while coming from four different geographical locations on the Moon and having different REE concentrations in their bulk-rock, do not exhibit any significant variations among their $\delta^{37}$Cl values (i.e. average olivine- and pyroxene-hosted MI $11.2 \pm 1.7$‰—Fig. 6). Finally, it has been recently highlighted that some high-Ti basalts don't fall on the same trend (Barnes et al., 2019), as well as high-Al basalts (Potts et al., 2018), probably indicating multiple and isotopically distinct Cl lunar reservoirs (Boyce et al., 2018) or post-crystallization processes (Potts et al., 2018—previous subsection). All these arguments suggest that, while heavier Cl isotopic signature of low-K and low-Ti basalts seems to correlate with KREEP signature, as apatites do, other processes need to be considered, such as metasomatism, to explain the chlorine isotopic values of MI from other types of mare basalts. Based on analyses of olivine- and pyroxene-hosted MI, and comparison with apatite literature data, we have strong evidence that the elevated $\delta^{37}$Cl of low-K and low-Ti lunar basalts is mainly inherited from the parent melt and not largely driven by magmatic processes during crystallization and subsequent eruption of the basalts. The heavy Cl isotopic signature of the Moon was acquired during the earliest stages of the LMO evolution, which may have be the time of a whole-scale evaporation as suggested by other volatile isotopic systems and abundances (Day and Moynier, 2014).

## 5. Conclusion

Apprehending the origin and evolution of Cl systematics of lunar samples is important in order to assess the Moon's volatile budget, which has further implications for the differentiation history of the Earth–Moon system. Olivine- and pyroxene-hosted MI from Apollo 10020, 12004, 12040 and 15016 lunar basalts exhibit Cl isotopic composition similar to the range observed for apatite from Apollo mare basalts measured previously. This is considered as a strong evidence that fractionated Cl isotopic signatures of mare magmas were established before their eruption and emplacement on the lunar surface. The corollary is that no significant Cl isotopic fractionation occurred between the melt-generation in the lunar mantle and during its journey towards the lunar surface and its ultimate solidification. However, there is evidence that in some cases, additional processes did influence the Cl isotopic composition of the lunar melts, especially towards the end stages of their crystallisation as is evident for Apollo 14 high-Al basalt in which MI seemed to have preserved the lunar mantle signature whereas apatite recorded the effect of later processes. Given the limited dataset on Cl isotopes in lunar MI, it is not possible to fully evaluate or verify the previously proposed hypothesis of mixing between a lighter basaltic reservoir and a $^{37}$Cl-rich KREEP reservoir and, therefore, in the near term, additional measurements on MI from KREEP-rich samples are required to address this issue. In the longer term, new MI measurements in samples collected from other areas of the Moon, not sampled by the Apollo missions (e.g. farside, polar regions etc.) could provide complementary data for developing a global-scale understanding of the history and evolution of volatiles in the Moon.

## Acknowledgements

We thank NASA CAPTEM for allocation of Apollo samples. The reviewers and associate editor are thanked for their insightful feedback and suggestions. This research was supported by a STFC grant to MA and IAF (#ST/I001964/1 and #ST/L000776/1).

## Appendix A. Supplementary material

Supplementary material related to this article can be found online at https://doi.org/10.1016/j.epsl.2019.115715.

## References

Albarede, F., Albalat, E., Lee, C.-T.A., 2015. An intrinsic volatility scale relevant to the Earth and Moon and the status of water in the Moon. Meteorit. Planet. Sci. 50 (4), 568–577.

Anders, E., Grevesse, N., 1989. Abundances of the elements: meteoritic and solar. Geochim. Cosmochim. Acta 53, 197–214.

Armytage, R.M.G., Georg, R.B., Williams, H.M., Halliday, A.N., 2012. Silicon isotopes in lunar rocks: implications for the Moon's formation and the early history of the Earth. Geochim. Cosmochim. Acta 77, 504–514.

Barnes, J.J., Tartèse, R., Anand, M., McCubbin, F.M., Neale, C.R., Franchi, I.A., 2016. Early degassing of lunar urKREEP by crust-breaching impact(s). Earth Planet. Sci. Lett. 447, 84–94.

Barnes, J.J., Franchi, I.A., Anand, M., Tartèse, R., Starkey, N.A., Koike, M., Sano, Y., Russell, S.S., 2013. Accurate and precise measurements of the D/H ratio and hydroxyl content in lunar apatites using. NanoSIMS. Chem. Geol. 337–338, 48–55.

Barnes, J.J., Franchi, I.A., McCubbin, F.M., Anand, M., 2019. Multiple volatile reservoirs in the lunar interior revealed by the isotopic composition of chlorine in lunar basalts. Geochim. Cosmochim. Acta. https://doi.org/10.1016/j.gca.2018.12.032. In press.

Barrett, T.J., Barnes, J.J., Anand, M., Franchi, I.A., Greenwood, R.C., Charlier, B.L.A., Zhoa, X., Moynier, F., Grady, M.M., 2019. Investigating magmatic processes in the early Solar System using the Cl isotopic systematics of eucrites. Geochim. Cosmochim. Acta. https://doi.org/10.1016/j.gca.2019.06.024. In press.

Beaty, D.W., Albee, A.L., 1978. Comparative petrology and possible genetic relations among Apollo 11 basalts. In: Proceedings of the 9th Lunar and Planetary Science Conference, pp. 359–463.

Bonifacie, M., Jendrzejewski, N., Agrinier, P., Humler, E., Coleman, M., Javoy, M., 2008. The chlorine isotope composition of the Earth's mantle. Science 319, 1518–1520.

Boyce, J.W., Treiman, A.H., Guan, Y., Ma, C., Eiler, J.M., Gross, J., Greenwood, J.P., Stolper, E.M., 2015. The chlorine isotope fingerprint of the lunar magma ocean. Sci. Adv. 1 (8).

Boyce, J.W., Kanee, S.A., McCubbin, F.M., Barnes, J.J., Bricker, H., Treiman, A.H., 2018. Early loss, fractionation, and redistribution of chlorine in the Moon as revealed by the low-Ti lunar mare basalt suite. Earth Planet. Sci. Lett. 500, 205–214.

Bucholz, C.E., Gaetani, G.A., Behn, M.D., Shimizu, N., 2013. Post-entrapment modification of volatiles and oxygen fugacity in olivine-hosted melt inclusions. Earth Planet. Sci. Lett. 374, 145–155.

Cannatelli, C., Doherty, A.L., Esposito, R., Lima, A., De Vivo, B., 2016. Understanding a volcano through a droplet: a melt inclusion approach. J. Geochem. Explor. 171, 4–19.

Canup, R.M., 2012. Forming a Moon with an Earth-like composition via a giant impact. Science. https://doi.org/10.1126/science.1226073.

Canup, R.M., Visscher, C., Salmon, J., Fegley Jr., B., 2015. Lunar volatile depletion due to incomplete accretion within an impact-generated disk. Nat. Geosci. 8, 918–921.

Chen, Y., Zhang, Y., Liu, Y., Guan, Y., Eiler, J., Stolper, E.M., 2015. Water, fluorine, and sulfur concentrations in the lunar mantle. Earth Planet. Sci. Lett. 427, 37–46.

Clog, M., 2010. Concentration et composition isotopique de l'hydrogene dans le manteau terrestre. Ph.D. thesis.

Cuk, M., Steward, S.T., 2012. Making the Moon from a fast-spinning Earth: a giant impact followed by resonant despinning. Science 338 (6110), 1047–1052.

Danyushevsky, L.V., McNeill, A.W., Sobolev, A.V., 2002. Experimental and petrological studies of melt inclusions in phenocrysts from mantle-derived magmas: an overview of techniques, advantages and complications. Chem. Geol. 183, 5–24.

Danyushevsky, L.V., Plechov, P., 2011. Petrolog3: integrated software for modelling crystallization processes. Geochem. Geophys. Geosyst. 12, 7.

Dauphas, N., Burkhardt, C., Warren, P.H., Fang-Zhen, F., 2014. Geochemical argumentsfor an Earth-like Moon-forming impactor. Philos. Trans. R. Soc. A 372, 20130244.

Day, M.D., Moynier, F., 2014. Evaporative fractionation of volatile stable isotopes and their bearing on the origin of the Moon. Philos. Trans. R. Soc. A 372, 20130259.

Esposito, R., Klebesz, R., Bartoli, O., Klyukin, Y.I., Moncada, D., Doherty, A.L., Bodnar, R.J., 2012. Application of the Linkam TS1400XY heating stage to melt inclusion studies. Cent. Eur. J. Geosci. 4 (2), 208–218.

Frezzotti, M.-L., 2001. Silicate-melt inclusions in magmatic rocks: applications to petrology. Lithos 55, 273–299.

Gaetani, G.A., O'Leary, J.A., Shimizu, N., Bucholz, C.E., Newville, M., 2012. Rapid reequilibration of $H_2O$ and oxygen fugacity in olivine-hosted melt inclusions. Geology 40 (10), 915–918.

Giesting, P.A., Schwenzer, S.P., Filiberto, J., Starkey, N.A., Franchi, I.A., Treiman, A.H., Tindle, A.G., Grady, M.M., 2015. Igneous and shock processes affecting chassignite amphibole evaluated using chlorine/water partitioning and hydrogen isotopes. Meteorit. Planet. Sci. 50, 433–460.

Greenwood, R.C., Barrat, J.-A., Miller, M.F., Anand, M., Dauphas, N., Franchi, I.A., Sillard, P., Starkey, N.A., 2018. Oxygen isotopic evidence for accretion of Earth's water before a high-energy Moon-forming giant impact. Sci. Adv. 4 (5928), 1–8.

Hallis, L.J., Anand, M., Greenwood, R.C., Miller, M.F., Franchi, I.A., Russell, S.S., 2010. The oxygen isotope composition, petrology and geochemistry of mare basalts: evidence for large-scale compositional variation in the lunar mantle. Geochim. Cosmochim. Acta 74, 6885–6899.

Hauri, E.H., 2002. SIMS analysis of volatiles in silicate glasses, 2: isotopes and abundances in Hawaiian melt inclusions. Chem. Geol. 183, 115–141.

Hauri, E.H., Weinreich, T., Saal, A.E., Rutherford, M.C., Van Orman, J.A., 2011. High pre-eruptive water contents preserved in lunar melt inclusions. Science 333 (6039), 213–215.

Jambon, A., Dhelle, B., Dreibus, G., Pineau, F., 1995. Chlorine and bromine abundance in MORB: the contrasting behaviour of the Mid-Atlantic Ridge and East Pacific Rise and implications for chlorine geodynamic cycle. Chem. Geol. 126, 101–117.

Kato, C., Moynier, F., Valdes, M.C., Dhaliwal, J.K., Day, J.M.D., 2015. Extensive volatile loss during formation and differentiation of the Moon. Nat. Commun. 6, 7617.

Kato, C., Moynier, F., 2017. Gallium isotopic evidence for extensive volatile loss from the Moon during its formation. Sci. Adv. 6, 7617.

Kaufman, R., Long, A., Bentley, H., Davis, S., 1984. Natural chlorine isotope variations. Nature 309, 338–340.

Kent, A.J.R., Elliott, T.R., 2002. Melt inclusions from Marianas arc lavas: implications for the composition and formation of island arc magmas. Chem. Geol. 183, 263–286.

Kleine, T., Palme, H., Mezger, K., Halliday, A.N., 2005. Hf-W chronometry of lunar metals and the age and early differentiation of the Moon. Science 310, 1671–1674.

Kramer, F.E., Twedell, D.B., Walton, W.J.A., 1977. Apollo 11 Lunar Sample Information Catalogue (revised). Curator's Office, JSC 12522.

Kruijer, T.S., Kleine, T., Fischer-Gödde, M., Sprung, P., 2015. Lunar tungsten isotopic evidence for the late veneer. Nature 520, 534–537.

Le Voyer, M., Asimow, P.D., Mosenfelder, J.L., Guan, Y., Wallace, P.J., Schiano, P., Stolper, E.M., Eiler, J.M., 2014. Zonation of $H_2O$ and F concentrations around melt inclusions in olivines. J. Petrol. 55 (4), 685–707.

Lowenstern, J.B., 2003. Melt inclusions come of age: volatiles, volcanoes, and sorby's legacy. In: Developments in Volcanology, vol. 5, pp. 1–21.

Manzini, M., Bouvier, A.-S., Barnes, J.D., Bonifacie, M., Rose-Koga, E.F., Ulmer, P., Metrich, N., Bardoux, G., Williams, J., Layne, G.D., Straub, S., Baumgartner, L.P., John, T., 2017. SIMS chlorine isotope.

McCubbin, F.M., Vander Kaaden, K.E., Tartese, R., Klima, R.L., Liu, Y., Mortimer, J., Barnes, J., Shearer, C.K., Treiman, A.H., Lawrence, D.J., Elardo, S.M., Hurley, D.M., Boyce, J.W., Anand, M., 2015. Magmatic volatiles (H, C, N, F, S, Cl) in the lunar mantle, crust, and regolith: abundances, distributions, processes, and reservoirs. Am. Mineral. 100 (8–9), 1668–1707.

Métrich, N., Wallace, P.J., Putirka, K.D., Tepley, F.J., 2008. Volatile abundances in basaltic magmas and their degassing paths tracked by melt inclusions. In: Minerals, Inclusions and Volcanic Processes. Rev. Mineral. Geochem. 69, 365–402. Mineralogical Society of America and Geochemical Society.

Meyer, C., 2009. Lunar sample compendium.

Moynier, F., Albarède, F., Herzog, G.F., 2006. Isotopic composition of zinc, copper, and iron in lunar samples. Geochim. Cosmochim. Acta 70, 6103–6117.

Newcombe, M.E., Fabbrizio, A., Zhang, Y., Ma, C., Le Voyer, M., Guan, Y., Eiler, J.M., Saal, A.E., Stolper, E.M., 2014.

Ni, P., Zhang, Y., Chen, S., Gagnon, J., 2019. A melt inclusion study on volatile abundances in the lunar mantle. Geochim. Cosmochim. Acta 249, 17–41.

Paniello, R.C., Day, J.M.D., Moynier, F., 2012. Zinc isotopic evidence for the origin of the Moon. Nature 490, 376–379.

Potts, N., Barnes, J.J., Tartese, R., Franchi, I.A., Anand, M., 2018. Chlorine isotopic compositions of apatite in Apollo 14 rocks: evidence for widespread vapor-phase metasomatism on the lunar nearside $\sim 4$ billion years ago. Geochim. Cosmochim. Acta 230, 46–59.

Pringle, E., Moynier, F., 2017. Rubidium isotopic composition of the Earth, meteorites, and the Moon: evidence for the origin of volatile loss during planetary accretion. Earth Planet. Sci. Lett. 473, 62–70.

Riciputi, L.R., Greenwood, J.P., 1998. Analysis of sulfur and carbon isotope ratios in mixed matrices by SIMS: implications for mass bias corrections. Int. J. Mass Spectrom. Ion Process. 178, 65–71.

Rhodes, J.M., Blanchard, D.P., 1980. Chemistry of Apollo 11 low-K mare basalts. In: Proceedings of the 11th Lunar and Planetary Science Conference, pp. 49–66.

Roedder, E., Weiblen, P.W., 1970. Lunar petrology of silicate melt inclusions, Apollo 11 rocks. In: Proceedings of the Apollo 11 Lunar Science Conference, vol. 1, pp. 801–837.

Roedder, E., Weiblen, P.W., 1971. Petrology of silicate melt inclusions, Apollo 11 and Apollo 12 and terrestrial equivalents. In: Proceedings of the Second Lunar Science Conference, vol. 1, pp. 507–528.

Roedder, E., 1979. Origin and significance of magmatic inclusions. Bull. Minéral. 102, 487–510.

Roedder, E., 1984. Occurrence and significance of magmatic inclusions and silicate liquid immiscibility. Acta Geol. Pol. 34 (1–2), 139–178.

Rubie, D.C., Jacobson, S.A., Morbidelli, A., O'Brien, D.P., Young, E.D., de Vries, J., Nimmo, F., Palme, H., Frost, D.J., 2015. Accretion and differentiation of the terrestrial planets with implications for the compositions of early-formed Solar System bodies and accretion od water. Icarus 248, 89–108.

Saal, A.E., Hauri, E.H., Langmuir, C.H., Perfit, M.R., 2002. Vapour undersaturation in primitive mid-ocean-ridge basalt and the volatile content of Earth's upper mantle. Nature 419, 451–455.

Saal, A.E., Hauri, E.H., Cascio, M.L., Van Orman, J.A., Rutherford, M.C., Cooper, R.F., 2008. Volatile content of lunar volcanic glasses and the presence of water in the Moon's interior. Nature 454 (7201), 192–195.

Saal, A.E., Hauri, E.H., Van Orman, J.A., Rutherford, M.J., 2013. Hydrogen isotopes in lunar volcanic glasses and melt inclusions reveal a carbonaceous chondrite heritage. Science 340, 1317–1320.

Sharp, Z.D., Barnes, J.D., Brearley, A.J., Chaussidon, M., Fischer, T.P., Kamenetsky, V.S., 2007. Chlorine isotope homogeneity of the mantle, crust and carbonaceous chondrites. Nature 446, 1062–1065.

Sharp, Z.D., Shearer, C.K., McKeegan, K.D., Barnes, J.D., Wang, Y.Q., 2010. The chlorine isotope composition of the Moon and implications for an anhydrous mantle. Science 329, 1050–1053.

Sharp, Z.D., Draper, D.S., 2013. The chlorine abundance of Earth: implications for a habitable planet. Earth Planet. Sci. Lett. 369–370, 71–77.
Sharp, Z.D., et al., 2013. The chlorine isotope composition of chondrites and Earth. Geochim. Cosmochim. Acta 107, 189–204.
Singer, J.A., Greenwood, J.P., Itoh, S., Sakamoto, N., Yurimoto, H., 2017. Evidence for the solar wind in lunar magmas: a study of slowly cooled samples of the Apollo 12 olivine basalt suite. Geochem. J. 51, 95–104.
Spicuzza, M.J., Day, J.M.D., Taylor, L.A., Valley, J.W., 2007. Oxygen isotope constraints on the origin and differentiation of the Moon. Earth and Planetary Science Letters 253, 254–265.
Steele-MacInnis, M., Esposito, R., Bodnar, R.J., 2011. Thermodynamic model for the effect of post-entrapment crystallization on the $H_2O$-$CO_2$ systematics of vapor-saturated, silicate melt inclusions. J. Petrol. 52 (12), 2461–2482.
Tartèse, R., Anand, M., Barnes, J.J., Starkey, N.A., Franchi, I.A., Sano, Y., 2013. The abundance, distribution, and isotopic composition of hydrogen in the Moon as revealed by basaltic lunar samples: implications for the volatile inventory of the Moon. Geochim. Cosmochim. Acta 122, 58–74.
Tartèse, R., Anand, M., Joy, K.H., Franchi, I.A., 2014. H and Cl isotope systematics of apatite in brecciated lunar meteorites Northwest Africa 4472, Northwest Africa 773, Sayh al Uhaymir 169, and Kalahari 009. Meteorit. Planet. Sci. 49 (12), 2266–2269.
Taylor, L.A., Patchen, A., Mayne, R.G., Taylor, D.-H., 2004. The most reduced rock from the Moon, Apollo 14 basalt 14053: its unique features and their origin. Am. Mineral. 89, 1617–1624.
Tikoo, S.M., Weiss, B.P., Buz, J., Lima, E.A., Shea, E.K., Melo, G., Grove, T.L., 2012. Magnetic fidelity of lunar samples and implications for an ancient core dynamo. Earth Planet. Sci. Lett. 337–338, 93–103.
Treiman, A.H., Boyce, J.W., Gross, J., Guan, Y., Eiler, J.M., Stolper, E.M., 2014. Phosphate-halogen metasomatism of lunar granulite 79215: impact-induced fractionation of volatiles and incompatible elements. Am. Mineral. 99, 1860–1870.
Usui, T., Alexander, C.M.O'D., Wang, J., Simon, J.I., Jones, J.H., 2012. Origin of water and mantle-crust interactions on Mars inferred from hydrogen isotopes and volatile element abundances of olivine-hosted melt inclusions of primitive shergottites. Earth Planet. Sci. Lett. 357–358, 119–129.
Walker, D., Longhi, J., Kirkpatrick, R.J., Hays, J.F., 1976. Differentiation of an Apollo 12 pricrite magma. In: Proceedings of the 7th Lunar Science Conference, pp. 1365–1389.
Wang, K., Jacobsen, S.B., 2016. Potassium isotopic evidence for a high-energy giant impact origin of the Moon. Nature 538, 487–490.
Webster, J.D., Tappen, C.M., Mandeville, C.W., 2009. Partitioning behavior of chlorine and fluorine in the system apatite–melt–fluid. II: felsic silicate systems at 200 MPa. Geochim. Cosmochim. Acta 73, 559–581.
Wiechert, U., Halliday, A.N., Lee, D.C., Snyder, G.A., Taylor, L.A., Rumble, D., 2001. Oxygen isotopes and the Moon-forming giant impact. Science 294, 345–348.
Young, E.D., Kohl, E.I., Warren, P.H., Rubie, D.C., Jacobson, S.A., Morbidelli, A., 2016. Oxygen isotopic evidence for vigorous mixing during the Moon-forming giant impact. Science 351, 493–496.
Zhang, J., Dauphas, N., Davis, A.M., Leya, I., Fedkin, A., 2012. The proto-Earth as a significant source of lunar material. Nat. Geosci. 5, 251–255.